Vol 16 No 9, September 2007
1009-1963/2007/16(09)/2803-06

Chinese Physics

© 2007 Chin. Phys. Soc.
and IOP Publishing Ltd

High density Al_2O_3/TaN-based metal–insulator–metal capacitors in application to radio frequency integrated circuits*

Ding Shi-Jin(丁士进)†, Huang Yu-Jian(黄宇健), Huang Yue(黄 玥), Pan Shao-Hui(潘少辉), Zhang Wei(张 卫), and Wang Li-Kang(汪礼康)

State Key Laboratory of ASIC and System, Department of Microelectronics, Fudan University, Shanghai 200433, *China*

(Received 18 October 2006; revised manuscript received 5 December 2006)

Metal–insulator–metal (MIM) capacitors with atomic-layer-deposited Al_2O_3 dielectric and reactively sputtered TaN electrodes in application to radio frequency integrated circuits have been characterized electrically. The capacitors exhibit a high density of about 6.05 fF/μm^2, a small leakage current of 4.8×10^{-8} A/cm^2 at 3 V, a high breakdown electric field of 8.61 MV/cm as well as acceptable voltage coefficients of capacitance (VCCs) of 795 ppm/V^2 and 268 ppm/V at 1 MHz. The observed properties should be attributed to high-quality Al_2O_3 film and chemically stable TaN electrodes. Further, a logarithmically linear relationship between quadratic VCC and frequency is observed due to the change of relaxation time with carrier mobility in the dielectric. The conduction mechanism in the high field ranges is dominated by the Poole–Frenkel emission, and the leakage current in the low field ranges is likely to be associated with trap-assisted tunnelling. Meanwhile, the Al_2O_3 dielectric presents charge trapping under low voltage stresses, and defect generation under high voltage stresses, and it has a hard-breakdown performance.

Keywords: metal–insulator–metal, atomic-layer-deposition, Al_2O_3, radio frequency integrated circuit

PACC: 7340R, 7360H

1. Introduction

With the rapid development of wireless and nanoscale devices, there is a strong demand for the decoupling and filtering of metal–insulator–metal (MIM) capacitors integrated within the back-end-of-line for integrated circuit manufacturing. The motivation to develop MIM capacitors, rather than conventional polysilicon capacitors, is to improve radio frequency performances due to their reduced substrate parasitic capacitance, low voltage coefficients, and high quality factor.[1,2] In order to minimize the capacitor area, thus increase the circuit density, the embedded MIM capacitors with a higher capacitance density are desired in the next generation of technology,[3] which can be implemented by employing either thinner insulators or high-permittivity (high-κ) insulators. However, the leakage current and reliability issues restrict the aggressive insulator thickness scaling down in the case of conventional silicon oxide ($\kappa =\sim 4$) and nitride dielectrics ($\kappa = 7$),[1] and the high-κ insulator is therefore considered as one of the most promising solutions.

In recent years, various deposition techniques for preparing high-κ films have been developed, such as ion-beam sputtering,[4] laser molecular beam epitaxy,[5] reactive radio frequency co-sputtering[6] and so on. However, for fabricating high-κ dielectric MIM capacitors, the main techniques include reactive sputtering,[7] atomic layer deposition (ALD),[8,9] pulsed laser deposition[10] and post-deposition oxidation (PDO) of metal.[11] Owing to the requirement for the MIM capacitors to be embedded into the interlevel dielectric layers, the maximum fabrication temperature should be compatible with the thermal budget ($< 450\,^\circ$C) of Cu back-end-of-line process. However, in the above temperature range, it is difficult to acquire such high-quality dielectrics by the reactive

*Project supported by the National Natural Science Foundation of China (Grant No 90607023), Shanghai Pujiang Program (Grant No 05PJ14017), SRF for ROCS, SEM, and the Micro/Nano-electronics Science and Technology Innovation Platform (985) and the Ministry of Education of China in the International Research Training Group "Materials and Concepts for Advanced Interconnects".

†Corresponding author. E-mail: sjding@fudan.edu.cn

sputtering or PDO of metal. The resulting films usually contain a large number of atomic vacancies, thus leading to a large leakage current and low breakdown strength.[7,11] With regard to the PLD technique, the deposited films encounter a major issue of surface morphology control as well as poor uniformity over a large area due to heavily fluctuating evaporation rate.[12] Recently, the ALD technique has attracted more and more attention on account of its various outstanding advantages, including the exquisite control of the film composition, high film uniformity, perfect conformity with high aspect ratio trench and low thermal budget,[13] thus it is significant to investigate the ALD high-κ dielectrics used in MIM capacitors.

High-κ Al_2O_3 material has a large band gap of 8.7 eV, a dielectric constant ($\kappa = 9$) higher than those of SiO_2 and Si_3N_4, and a compact and amorphous texture under the conditions of interest,[14] therefore, we have investigated intensively atomic-layer-deposited Al_2O_3 films as gate dielectrics for silicon- and GaAs-based metal–oxide–semiconductor devices.[15,16] In addition, the atomic-layer-deposited Al_2O_3 dielectric has also been examined in application of Al_2O_3/Ta-based MIM capacitor to radio frequency and mixed-signal integrated circuits. However, the achieved capacitance density is as small as 2.2 fF/μm^2, with the leakage current retaining an acceptable level.[9] In this article, we report on the use of very thin (13 nm) Al_2O_3 film as an insulator of the MIM capacitor fabricated by ALD together with TaN electrodes. The fabricated MIM capacitor exhibits a significantly enhanced capacitance density, low leakage current, and high breakdown strength.

2. Experiments

A one-quarter 15.2 cm diameter silicon wafer was used as a starting substrate. Firstly, an about 400 nm thick SiO_2 layer was grown on a silicon wafer by low-pressure thermal chemical vapour deposition of $Si(OC_2H_5)_4$, followed by the deposition of an about 150 nm thick TaN layer as a bottom electrode by reactively sputtering a Ta target in the ambient of N_2/Ar at a flow rate ratio of 1:5 and a working pressure of 0.4 Pa, with a DC power of 450 W applied to the target, and an RF power of 12 W, to the substrate. Subsequently, the TaN-coated wafer was transferred into an ALD chamber for Al_2O_3 deposition. In the present experiment, a 13 nm thick Al_2O_3 film was deposited by using H_2O and $Al(CH_3)_3$ precursors at 320°C. After the dielectric deposition, the same thick TaN film was prepared as a top electrode, followed by annealing at 420 °C in the forming gas (95%-N_2 and 5%-H_2) for 30 min. Finally, a photolithography step was carried out to make a capacitor pattern with a size of 100 μm×100 μm, followed by etching the top metal and the insulator in Cl_2 gas atmosphere at an initial substrate temperature of 60 °C. Subsequently, the block resist was removed by O_2 plasma. Capacitance–voltage ($C-V$) measurements were performed by using a precise LCR meter (HP4284A) with a 25 mV ac sweeping signal. Current–voltage ($I-V$) characteristics were measured using a semiconductor parameter analyser (HP4155B).

3. Results and discussion

Figure 1 shows the capacitance density and dissipation factor of the MIM capacitor as a function of frequency at zero-bias. It is found that the capacitance density does not present an evident variation with frequency increasing, which is in a range of 5.77–6.02 fF/μm^2 for the applied frequencies between 1 kHz and 1 MHz. Although the dissipation factor of the capacitor exhibits a rise in the case of the frequency higher than 100 kHz, we do not observe a decrease in the capacitance density. This may be due to an exposure of the sample to the ambient prior to the electrical measurements, leading to adsorptions of water, etc on the sample surface. The inset in Fig.1 shows the

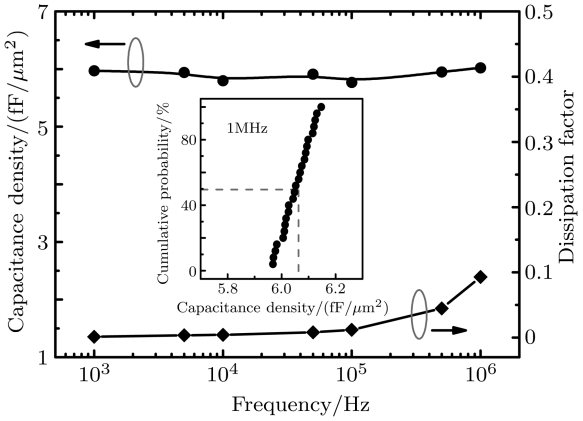


Fig.1. Dependences of capacitance density and dissipation factor on the applied frequency at zero-bias. The inset shows the distribution of the capacitance densities at 0V and 1MHz.

capacitance–density distribution of the capacitor on the same wafer, suggesting a mean capacitance den-

sity of 6.05 fF/μm^2, which is much higher than the achieved value (1.2−2.8 fF/μm^2) in the case of conventional Si_3N_4 dielectric.[17] Moreover, the compact distribution of capacitance densities (a distribution width of 0.18 fF/μm^2) indicates that the ALD Al_2O_3 film is very uniform. According to a parallel plate capacitor model, $C = \varepsilon_0\kappa A/d$, and the calculated relative dielectric constant of Al_2O_3 equals 8.9, which is in good accordance with that reported in Ref.[14].

Voltage coefficients of capacitance (VCCs) are very important parameters in the application of MIM capacitors to radio frequency circuits, and can be determined by using the following equation to fit the experimental data:[8]

$$C(V) = C_0(\alpha V^2 + \beta V + 1),$$

where C_0 is the capacitance at zero bias; α and β represent quadratic and linear VCCs, respectively. To obtain VCCs, normalized capacitance (C_V/C_0) versus dc bias is plotted in Fig.2 at three different frequencies, and the extracted VCCs are also presented. It

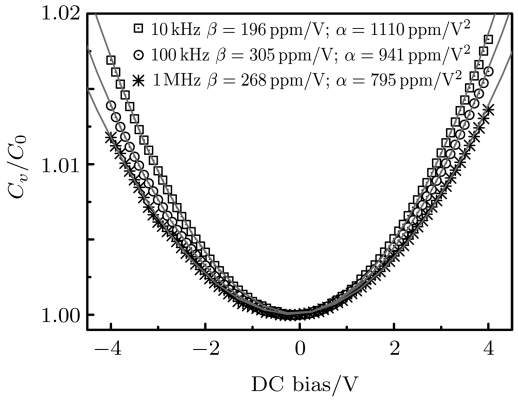


Fig.2. Normalized capacitance (C_V/C_0) versus dc bias at frequencies of 10 k, 100 k and 1 MHz, separately. The extracted α and β for different frequencies are also presented. The discontinuous symbols represent the original data at different frequencies, and the solid lines denote the fitting curves.

is found that α decreases monotonically from 1110 ppm/V^2 to 795 ppm/V^2 as the applied frequency increases from 10 kHz to 1 MHz. However, β does not exhibit the aforementioned change. In order to comprehensively observe frequency-dependences of α and β values, we have measured C–V curves at more frequencies. The extracted α values are plotted as a function of frequency as indicated in Fig.3, where a logarithmically linear relationship is obtained between α and frequency. The aforementioned frequency-dependence of α is also observed in the high-κ HfO_2 MIM capacitors, and is explained as the fact that the carrier mobility becomes smaller with increasing frequency, which leads to a longer relaxation time and a smaller variation in capacitance.[18] Furthermore, the extracted β values are also plotted as a function of frequency as shown in the inset of Fig.3. It can be seen that β does not exhibit any regular variation with frequency.

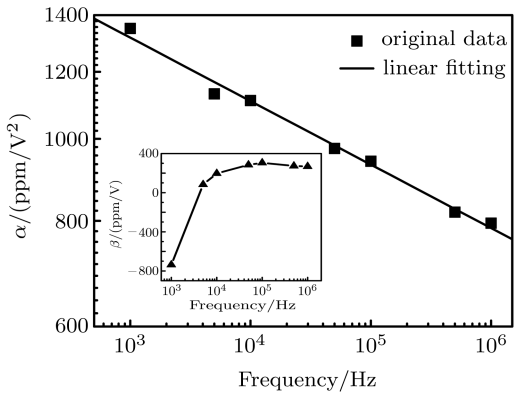


Fig.3. Quadratic VCC (α) versus frequency in a logarithm-logarithm scale. The inset shows linear VCC (β) versus frequency.

Figure 4 shows the typical $I-V$ characteristic curve of the capacitor, indicating a leakage current density lower than 1×10^{-7} A/cm^2 in the range of $-4 \sim +4$ V. Further, we can see that the leakage current at 3 V is as small as 4.8×10^{-8} A/cm^2. It is worth indicating that the forming gas anneal (FGA) prior to the formation of capacitors is helpful to reducing the leakage current, as reported by Kim *et al*[7] and Lin *et al.*[19] This is most likely attributed to the following two factors.[19] The FGA leads to the formation of a thermodynamically stable bonded interface with good interface properties. On the other hand, the weak Al–O bond can readily be broken in a reducing gas during the FGA, but the top metal film prevents O species desorption from forming the Al_2O_3 film. Therefore, a dynamic equivalent process must occur inside the isolated Al_2O_3 system, and at last form the stable Al–O bond of the Al_2O_3 system. Additionally, the symmetrical $I-V$ curve reveals comparable interfacial properties of dielectric/electrode. The breakdown strength of the MIM capacitor generally reflects the device lifetime, therefore, for obtaining the breakdown-electric-field (E_{BD}) of the capacitor, a continuously incremental voltage is applied to the MIM capacitor till electrical breakdown. The inset in Fig.4 presents a cumulative distribution of E_{BD}. It is found that the E_{BD}

amounts to 8.61 MV/cm in the case of 50% breakdown probability, such a high E_{BD} is useful to enhancing the device lifetime.

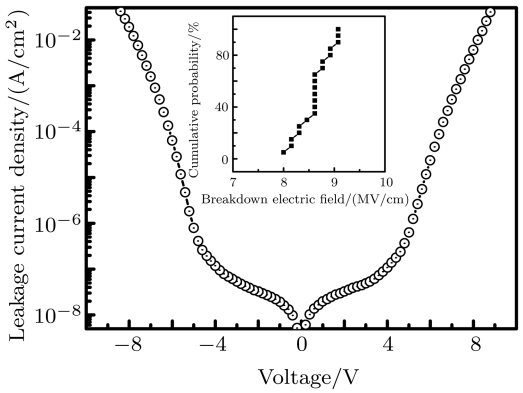


Fig.4. Dependence of leakage current density on voltage. The inset shows cumulative distribution of breakdown electric fields of the MIM capacitors.

For an understanding of the possible conduction mechanisms occurring in the current MIM capacitor, the $I-V$ curves are plotted according to the Poole–Frenkel (P–F) emission and Schottky emission, respectively. Figure 5(a) shows $\ln(J/E)$ versus $E^{1/2}$ due to the P–F emission. It is evident that a straight line is achieved in high electric-field ranges. According to the slope of the straight line, the deduced refractive index (n) is 1.8, which is close to the experimental value (1.68) for Al_2O_3 layer prepared by plasma assisted atomic layer deposition.[20] However, if we fit the same data using the Schottky emission (not shown here), the resulting refractive index is as small as 0.86, which is far from the measured one. Accordingly, it is reasonable that the conduction mechanism in high electric-field ranges is dominated by the P–F emission. In addition, it is well known that the Schottky emission usually occurs at lower electric fields, and $\ln J$ is thus plotted as a function of $E^{1/2}$ according to the Schottky emission as shown in Fig.5(b). The extracted refractive index is about 10, which deviates severely from the experimental one. This reveals that the Schottky emission is not dominant in the low electric-field ranges. Considering that the Al_2O_3 film contains a lot of traps, the leakage current at the lower electric fields is likely to be associated with the trap-assisted tunnelling.

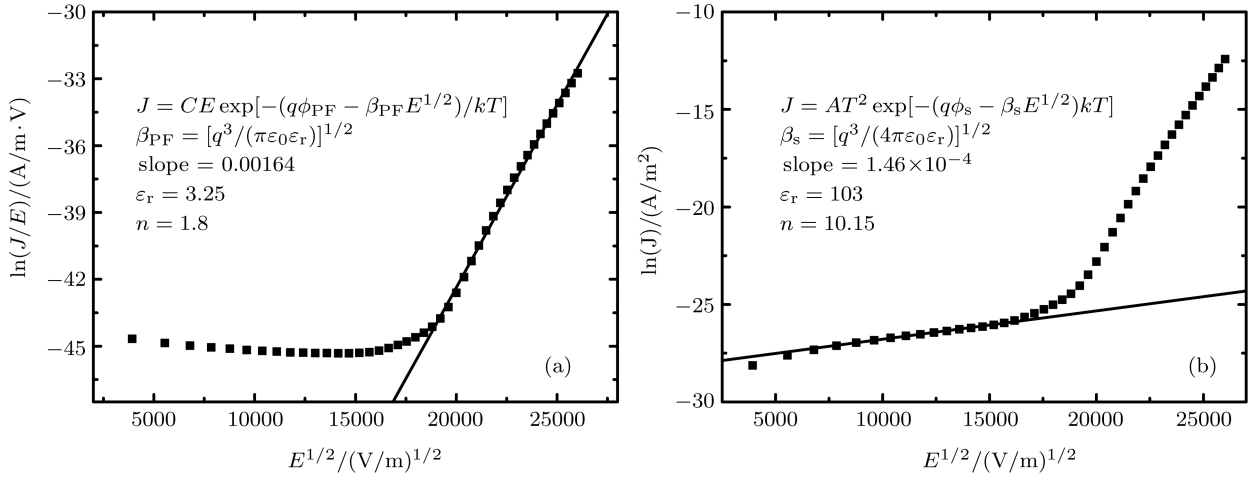


Fig.5. $\ln(J/E)$ versus $E^{1/2}$ together with a fitted straight line in high electric field ranges (a) where the inserted formula describes the Poole–Frenkel emission, C is a constant, ϕ_{PF} is the barrier height separating the traps from the conduction band, and $\ln J$ versus $E^{1/2}$ together with a fitted straight line in the low electric field ranges (b). The Schottky emission is described by the inserted formula, where A is the effective Richardson constant, ϕ_s represents the barrier height between the injecting electrode and the dielectric material. In the aforementioned two formulas, ε_r denotes the high frequency permittivity of the material and equals the square of the refractive index ($\varepsilon_r = n^2$); ε_0, q and k represent the permittivity of free space, the electronic charge and the Boltzmann constant, respectively. The absolute temperature T equals 298K in our case.

Table 1 shows a comparison of the present results with other reported ones on Al_2O_3 MIM capacitors. Compared with our ALD Al_2O_3 film, the post-deposition oxidation of Al film offers much larger leakage current density and a lower capacitance density as well. This should be attributed to the fact that the Al film cannot be oxidized completely under the experimental condition (for instance, 400 °C), thus result-

ing in the formation of non-stoichiometric Al_2O_3 film. Therefore, the resulting film contains a number of oxygen vacancies, which favours the leakage characteristic of the Al_2O_3 film. By using Ta electrodes, the oxidation of the Ta bottom electrode easily occurs during atomic layer deposition of Al_2O_3 due to its exposure to the water and thermal ambient, which can be reflected by Gibbs energy of formation ($\sim -298.76\,\mathrm{kJ/mol}$) for Ta_2O_5, so the interfacial layer with inferior quality is formed. This will cause the decrease in the capacitance density. In a word, our fabricated MIM capacitor exhibits the highest capacitance density while retaining a minimal leakage current, which is related to not only a high-quality atomic-layer-deposited Al_2O_3 insulator but also more stable TaN electrodes.

Table 1. A comparison of our results with other reported ones on Al_2O_3 MIM capacitors.

reference	technology for preparing Al_2O_3 film	electrode material	capacitance density/(fF/μm^2)	leakage current density/(A/cm^2)
[11]	post-deposition oxidation of thin Al film	Pt bottom electrode; Al top electrode	5	2×10^{-7} at 2V
[9]	atomic-layer-deposition	Ta electrodes	2.2	4.9×10^{-8} at 3V
Our results	atomic-layer-deposition	TaN electrodes	6.05	4.8×10^{-8} at 3 V

Finally, the time characteristic for the capacitor to break down is measured under different constant voltage stresses as shown in Fig.6. Under constant voltage stresses of 4 V and 7 V, the leakage current density decreases monotonically with increasing stress time, which is due to a charge trapping effect.[21] The aforementioned characteristic may be very useful to obtaining a long lifetime of device. When the stress voltage is raised to 8V or higher, an increase in leakage current occurs in a range of longer stress time. This can be attributed to the trap-assisted leakage current due to defect generation under high voltage stresses. Further, a sudden and sharp rise of the leakage current can be observed, suggesting a hard-breakdown characteristic.

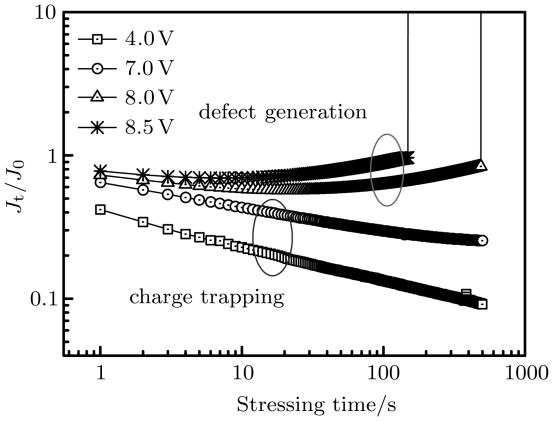


Fig.6. Evolution of normalized leakage current (J_t/J_0) with stress time under different constant voltage stresses. J_0 and J_t denote the leakage currents before the stress and after the stress time t, respectively.

4. Conclusions

The MIM capacitors have been fabricated by using an ALD Al_2O_3 insulator and sputtered TaN electrodes, exhibiting a high density of about $6.05\,\mathrm{fF}/\mu\mathrm{m}^2$, a small leakage current of 4.8×10^{-8} A/cm^2 at 3 V, a high E_{BD} of 8.61 MV/cm as well as acceptable quadratic VCC of $795\,\mathrm{ppm/V}^2$ and linear VCC of 268 ppm/V at 1 MHz. The observed properties should be attributed to high-quality Al_2O_3 film and chemically stable TaN electrodes. Furthermore, a logarithmically linear relationship between quadratic VCC and frequency is observed, which is correlated with the decrease in the carrier mobility with increasing frequency, thus leading to a higher relaxation time and a smaller capacitance variation. The conduction mechanism in high field ranges is dominated by the Poole–Frenkel emission, while the leakage current in low field ranges is very likely to be associated with trap-assisted tunnelling. Finally, the charge trapping and defect generation are demonstrated, respectively, under low voltage stresses and high voltage stresses. At the same time, a hard-breakdown characteristic of the MIM capacitor is also observed.

References

[1] Remmel T, Ramprasad R and Walls J 2003 *Proc. Int. Rel. Phys. Symp.* p277

[2] Kar-Roy A, Hu C, Racanelli M, Compton C A, Kempf P, Jolly G, Sherman P N, Zhang J and Yin A 1999 *Proc. IITC* p245

[3] *Radio Frequency and Analog/Mixed-Signal Technologies for Wireless Communications*, in 2005 *International Technology Roadmap for Semiconductors* (Semiconductor Industry Association, Palo Alto)

[4] Han D D, Kang J F, Lin C H and Han R Q 2003 *Chin. Phys.* **12** 325

[5] Xiang W F, Lu H B, Chen Z H, He M, Lu X B, Liu L F, Guo H Z and Zhou Y L 2005 *Chin. Phys. Lett.* **22** 182

[6] Guo D F, Geng W G, Lan W, Huang C M and Wang Y Y 2005 *Acta Phys. Sin.* **54** 5901 (in Chinese)

[7] Kim S J, Cho B J, Li M F, Yu X, Zhu C, Chin A and Kwong D L 2003 *IEEE Electron Device Lett.* **24** 387

[8] Ding S J, Zhu C, Li M F and Zhang D W 2005 *Appl. Phys. Lett.* **87** 053501

[9] Hu H, Zhu C, Yu X, Chin A, Li M F, Cho B J, Kwong D L, Foo P D, Yu M B, Liu X and Winkler J 2003 *IEEE Electron Device Lett.* **24** 60

[10] Hu H, Zhu C, Lu Y F, Li M F, Cho B J and Choi W K 2002 *IEEE Electron Device Lett.* **23** 514

[11] Chen S B, Lai C H, Chin A, Hsieh J C and Liu J 2002 *IEEE Electron Device Lett.* **23** 185

[12] Houssa M 2004 *High-κ Gate Dielectrics* (Bristol: IOP Publishing), p89, p107

[13] Hausmann D, Becker J, Wang S and Gordon R G 2002 *Science* **298** 402

[14] Wilk G D, Wallace R M and Anthony J M 2001 *J. Appl. Phys.* **89** 5243

[15] Xu M, Xu C H, Ding S J, Lu H L, Chen W, Zhang D W and Wang L K 2006 *J. Appl. Phys.* **99** 074109

[16] Lu H L, Sun L, Ding S J, Xu M, Zhang D W and Wang L K 2006 *Appl. Phys. Lett.* **89** 152910

[17] Bolam R J, Ramachandran V, Coolbaugh D and Watson K M 2003 *IEEE Trans. Electron Devices* **50** 941

[18] Zhu C, Hu H, Yu X, Kim S J, Chin A, Li M F, Cho B J and Kwong D L 2003 *Tech. Dig. Int. Electron Devices Meet.* p879

[19] Lin J, Suzuki T, Matsunaga D and Eguchi K 2006 *Appl. Phys. Lett.* **88** 062902

[20] Jeong C W, Lee B I and Joo S K 2001 *Mater. Sci. Eng.* C **16** 59

[21] Ding S J, Hu H, Zhu C, Kim S J, Yu X F, Li M F, Cho B J, Chan D S H, Rustagi S C, Yu M B and Chin A 2004 *IEEE Trans. Electron Devices* **51** 886